Test Method

The fracture testing of ductile polymer films: Effect of the specimen notching

N. León[a, *]

noel.leon@estudiant.upc.edu

A.B. Martínez[a]

P. Castejón[a]

D. Arencón[a]

P.P. Martínez[b]

[a]Centre Català del Plàstic, Departament de Ciència dels Materials i Enginyeria Metal-lúrgica, Universitat Politècnica de Catalunya, BarcelonaTech, C/Colom 114, 08222 Terrassa, Spain

[b]NUDEC SA, C/ Pintor Vila Cinca, 24-28, Pol. Ind. Can Humet de Dalt, 08213 Polinyà, Spain

*Corresponding author.

Abstract

The fracture of a ductile polymer film, a heterophase ethylene-propylene block copolymer, has been studied, combining a range of characterisation methods in an attempt to provide a better understanding of the intricate details that play an important role in the repeatability and reproducibility of the essential work of fracture test. The experimental factors that have a strong influence on the resulting parameters are clearly explained, with particular attention to the effect of the quality of the notches, the non-collinearity of the two edge notches in double edge notched tension specimens, and the lack of alignment of the specimen with the load axis once it is mounted on the load train. Furthermore, the influence of these experimental factors on the registered stress-displacement curves is also studied, and a criterion and the method for separating non-valid specimens are established.

Keywords: Fracture; Essential work of fracture; J-integral; Polymer film

1 Introduction

Polymer films are used in a wide variety of applications. Their toughness is often a basic requisite to meet some industry needs.

The Linear Elastic Fracture Mechanics (LEFM) approach is used to study fractures occurring at nominal stresses well below the material yield stress. The dissipated energy is confined in a small area near the crack tip, and the fracture is brittle. The LEFM approach is not applicable when the plasticity around the crack tip becomes large; in those cases the Elastic Plastic Fracture Mechanics (EPFM) is applied. When the crack propagation occurs through a highly deformed and yielded material then Post-Yield Fracture Mechanics can also be applied and the Essential Work of Fracture (EWF) is a suitable methodology.

The EWF approach has become very popular to characterise fracture of polymer films and is increasingly used due to its apparent simple preparation and easy testing. The EWF characterises the plane stress toughness in mode I, generally using the double edge notched tension (DENT) configuration for the specimens.

In spite of the apparent simplicity of the EWF test, some aspects of the validity of this technique remain controversial; there are intricate details that seem to play an important role in the repeatability and reproducibility of the test. This problem has been and still is a topic of much debate, and these questions indicate that the EWF procedure is not yet sufficiently well-defined to be standardised. Some of the aspects of the test validity are related to the specimen manufacture, particularly the quality of the notches.

Two sets of specimens have been prepared, the first one sharpened by the femtosecond laser ablation technique, and the second one sharpened by the classical razor blade sliding technique. These two sets of specimens have

been characterised by combining the EWF, J-integral, and crack tip opening displacement (CTOD) methods in an attempt to provide a better understanding of the EWF fracture approach for characterising the fracture toughness of a ductile polymer film. The connection between the quality of the notches and the shape and size of the registered stress-displacement curves has been established. This was done in order to find a criterion and a method to eliminate non-valid specimens. Furthermore, it has been studied in detail how the size and shape of the stress-displacement curves are related to the EWF fracture parameters.

The effect on the stress-displacement curves of specimens with non-collinear notches, specimens with different quality between the two edge notches, and specimens having a lack of alignment with the load axis once mounted on the testing machine grips have been also studied.

Moreover, there is a limited understanding of the polymers to which the EWF approach can be applicable. The EWF approach has been successfully applied to polymers that undergo necking before crack propagation. However, there is some controversy over the applicability of the EWF approach to heterophase polymers, which can deform by other mechanisms. For this reason, a very ductile grade of an ethylene-propylene block copolymer (EPBC), which is prone to plastic deformation and thus problematic for the notch sharpening, was tested.

The main objective of this work is to contribute to a better understanding and to clarify some of the controversial factors involved in the EWF test.

2 The EWF approach

2.1 The EWF concept

The EWF approach [1] is based on the hypothesis that the total energy involved during the ductile fracture of a pre-cracked specimen (W_f) can be separated into two terms.

$$W_f = W_e + W_p \quad \textbf{(1)}$$

where W_e, the essential work of fracture, represents the energy required for the creation of two new surfaces during the crack propagation, whereas the second term, W_p, is called the plastic work or the non-essential work of fracture and collects all other sources of energy produced throughout the fracture process. The term W_e is considered to be proportional to the area of the Fracture Process Zone (FPZ) while W_p is proportional to the volume of the Outer Plastic Zone (OPZ). These zones are schematised in Fig. 1 for a DENT specimen.

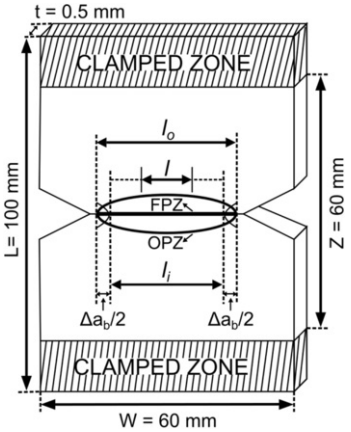

Fig. 1 DENT specimen geometry.

alt-text: Fig. 1

Rewriting Eq. (1) using specific terms,

$$w_f = \frac{W_f}{l_o g t} = w_e + \beta w_p \cdot l_o \quad \textbf{(2)}$$

where t is the specimen thickness, l_o is the original ligament length and β is a factor that depends on the shape of the OPZ.

It is possible to assess Eq. (2) by performing a series of tests on specimens with different ligament lengths, and subsequently plotting the specific total work of fracture values, w_f, as a function of their ligament lengths. A

simple regression analysis of this plot shows that the specific essential work of fracture, w_e, and the specific non-essential work of fracture, βw_p, are the intercept for a zero ligament length and the slope of the linear regression line, respectively.

The value which represents the toughness, namely, w_e, is an inherent material parameter only if the ligament yields fully before the onset of crack propagation.

2.2 Key assumptions

In the EWF analysis, the following three basic key assumptions are made:

a) The l_o is fully yielded prior to the onset of crack propagation.

In a DENT specimen, it could be estimated that l_o will be completely yielded prior to the onset of crack propagation if it is less than twice the size of the plastic zone radius, r_p. Under plane stress conditions, for a linear plastic zone

$$2r_p = \frac{\pi}{8}\left(\frac{Ew_e}{\sigma_y^2}\right) \quad \textbf{(3)}$$

and for a circular plastic zone

$$2r_p = \frac{Ew_e}{\pi\sigma_y^2} \quad \textbf{(4)}$$

where E is the elastic modulus and σ_y is the uniaxial yield stress.

Although having $l_o \leq 2r_p$ is a reasonable size criterion, it appears to be too restrictive.

b) Fracture occurs under plane stress conditions.

As polymer films have a thickness of less than 1 mm, a practical lower limit of 5 mm for l_o has been accepted when preparing DENT specimens to be properly handled. The upper limit for l_o requires full-ligament yielding before crack propagation. Hence, l_o has to be less than twice r_p in DENT specimens.

Another upper limit is given by the relationship:

$$l_o \leq \frac{W}{3} \quad \textbf{(5)}$$

where W is the specimen width. This last condition is necessary to prevent edge effects.

c) Good quality notches.

Good quality means identical and repetitive sharp notches without plastic deformation in front of the notch tip. This requirement guarantees self-similar load-displacement and ligament length-displacement curves for the tested specimens [2,3].

The notch sharpening is of critical importance in obtaining good results [4–6]. The larger notch tip radius or plastic deformation, the higher w_e values.

2.3 Other considerations

When the key assumptions are satisfied, w_e is the specific energy just before crack initiation. That is, an initiation value which coincides with the J-integral value at initiation, J_o [2].

Hill has demonstrated [7] that in the DENT geometry under plane stress conditions, no stress can exceed the value of 1.15 σ_y. Thus, the maximum stress registered during the DENT test, σ_{max}, has to be between σ_y and 1.15 σ_y, and its value is equal for all the ligaments. Theoretically, at small values of l_o, the specimen can be in a mixed state of stress, which increases σ_{max}. Therefore, this Hill criterion could be useful to determine the lower limit of l_o. In practice, the experimental variability in the σ_{max} values creates difficulties for the application of this criterion. Clutton [4] has suggested another criterion, which utilises the mean of the maximum stresses, where

$$0.9\sigma_{max} < \bar{\sigma}_{max} < 1 \cdot 1\sigma_{max} \quad (6)$$

This criterion only removes data where an error in dimensional measurement or in load exists.

3 Experimental details

3.1 Material

The study has been conducted on a commercial grade of EPBC. The microstructure consists [8] of elastomeric ethylene-propylene particles embedded in a polypropylene matrix.

Polypropylene requires improved toughness at both room and low temperatures to fulfil some industry requirements. The mechanism responsible for the toughness reinforcement is the formation of shear bands around the elastomeric particles, which absorbs most of the deformation energy.

The raw material in the form of pellets was kindly supplied by REPSOL. Films that were 0.5 mm thick were cast-extruded from the pellets.

3.2 Specimen preparation

Two kinds of specimens were prepared: dumbbell shaped and DENT specimens. All the specimens were prepared and tested in the machine direction orientation.

Dumbbell shaped specimens were obtained in a cutting press with the shape and dimensions of ISO 527-3 type V specimen.

The DENT specimens were used to perform the fracture tests. EPBC films were cut in rectangular coupons (Fig. 1), which were pre-notched forming saw cut slots. The notches had to be collinear, and placed opposite one another at the midpoint of the specimen height.

The most popular method used to sharpen notches is the razor blade sliding technique. In this technique, the notches are sharpened by drawing a fresh razor blade across the pre-notch. It is advisable to do this in a single pass so that the razor blade follows the same track, avoiding bifurcations. Instead of a razor blade, scalpels have also been used. Cooling the specimens below their glass transition temperature (T_g) prior to the sliding technique can be helpful. Very small notch tip radii of around 1 μm can be manufactured. Unintentional development of a plastic zone ahead of the notch tip can be induced by the compressive component of the sideways sliding force. The notch quality is depending on the technique used, and even on the operator skill.

The femtosecond pulsed laser ablation technique (femtolaser) can be used to micromachine practically any material, with negligible thermal damage to the surface surrounding the ablated areas. With proper set-up, this technique allows obtaining consistent notches that have negligible thermal damage, no plastic deformation, and a notch tip radius of approximately 1 μm [2,3,6].

The sharpening of the pre-notched EPBC specimens was carried out using two different methods, the femtolaser ablation technique and razor blade sliding.

In one set of 18 specimens, the machined pre-notch was extended by the application of the femtolaser ablation technique with the same set-up and other variables, as defined for another EPBC grade [6].

The second set of 18 specimens was sharpened by manually sliding a new razor blade across the pre-notch in a single pass.

The l_o of each specimen was measured after testing in an optical microscope.

One surface of each specimen was adequately sprayed with a speckle pattern before being tested.

3.3 Test conditions

All tests were carried out at 23 ± 1 °C using a crosshead speed of 2 mm/min on a Zwick servo-hydraulic testing machine, which was fitted with a two-camera digital image correlation (DIC) system and Aramis software (GOM, Germany).

In general, DIC is based on the principle of comparing speckle patterns on the surface of the deformed samples, or between any two deformation states. Surfaces with high contrast are required to avoid image distortion and therefore inaccurate data. Hence, before testing, one surface of each specimen was covered with a thin white coating before being sprayed in order to obtain black points, as required by the DIC system.

Uniaxial tensile tests were performed on the dumbbell shaped specimens. The load was registered by the load cell and the displacements by the DIC system.

The DENT specimens were tested, in mode I, until complete failure. The specimens were properly clamped with an original distance between clamps of Z = 60 mm. For each specimen, the load as a function of the cross-head displacement, d_z, was registered.

DIC system images obtained during the tests were recorded for all the specimens. These images were also analysed with the software for measuring the deformation and the ligament length evolution throughout the test. The displacement d_{opz} was measured with two reference points very near to each other, but outside the outer plastic zone, which corresponds to the largest l_o specimen. The distance between these two reference points was always the same for all specimens of a given set. Then, by using the registered loads, displacements, and ligament lengths, two sets of data, for each specimen, can be plotted. Specifically, the load is plotted as a function of the displacement, and the ligament length l as a function of the displacement.

4 Results and discussion

4.1 Uniaxial tensile test

The σ_y and E values of the EPBC film were measured on 5 dumbbell shaped specimens following the ISO standard 527, resulting in E = 1.24 ± 0.1 GPa and σ_y = 25.0 ± 0.2 MPa. The specimens showed a whitening zone in the deformed area, which is characteristic of the heterophase polymers.

4.2 Notch quality

The notches of two specimens from each set were observed by optical light microscopy and also by scanning electron microscopy (SEM).

Observation of the razor blade sharpened notches under the light microscope (Fig. 2a) revealed some stress whitening ahead of the notch tip, indicating that some plastic deformation had taken place. This phenomenon was not present in the notches of the femtolaser specimens (Fig. 2b).

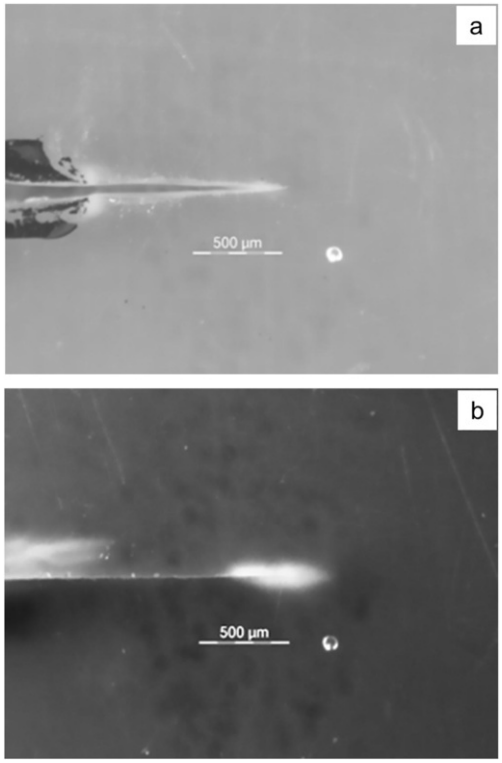

Fig. 2 Optical micrographs: a) Femtolaser notch, b) Razor blade notch.

alt-text: Fig. 2

The SEM micrographs of the razor blade notches (Fig. 3) revealed volume accumulation of plastically deformed material at the notch tip. The notch tip radius was less than 1 μm and the sharpening extension varied between 900 and 1300 μm.

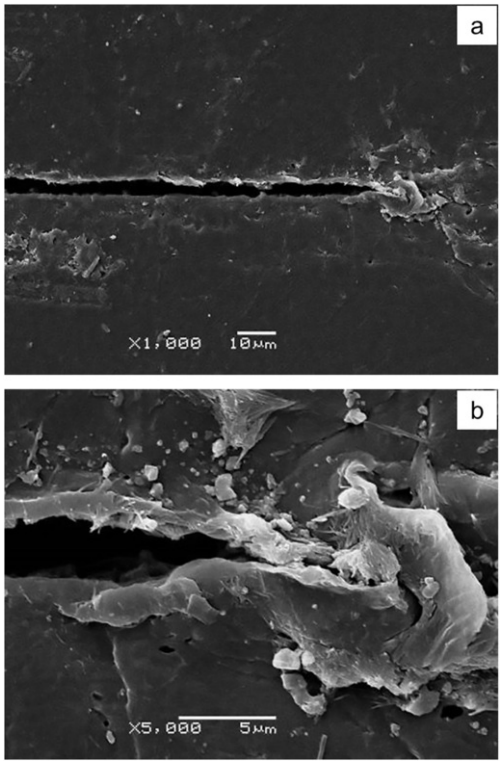

Fig. 3 SEM micrographs of a razor blade specimen: a) Extended notch, b) Notch tip detail.

alt-text: Fig. 3

All the femtolaser notches observed through the SEM turned out to be virtually identical (Fig. 4), with a notch tip radius less than 1 μm and a sharpening depth of 750 μm. It was also observed that there was no plastic deformation and negligible thermal damage at the notch root.

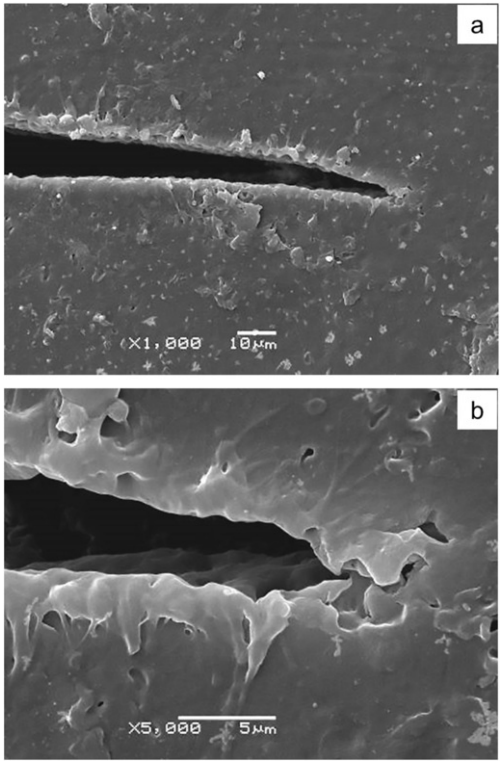

Fig. 4 SEM micrographs of a femtolaser notch: a) General view, b) Detail of the crack tip.

alt-text: Fig. 4

Both types of notches were very sharp, with practically the same notch tip radius, but there were differences in the plastic deformation at the notch root, which was visible in the razor blade notches and absent in the femtolaser ones.

The second phase particles of the EPBC act as stress concentrators, and so only a small compressive component of the sliding force is needed to produce plastic deformation, which is visualised as whitening.

4.3 Femtolaser specimens

The load versus displacement (d_{opz}) curves obtained through testing are represented in Fig. 5, for each one of the 16 specimens tested. Here, a partial overlap of the curves corresponding to l_o = 5.89 mm and l_o = 6.45 mm as well as the curves l_o = 19.37 mm and l_o = 20.39 mm can be observed.

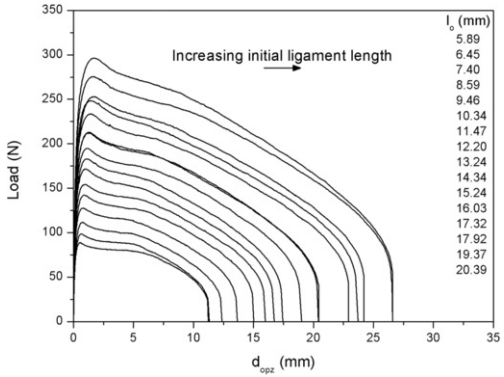

Fig. 5 Registered load-d_{opz} curves for the 16 femtolaser specimens.

alt-text: Fig. 5

The ligament lengths (l) as a function of the displacement (d_{opz}) are represented in Fig. 6 for the same 16 tested specimens. As in Fig. 5, a partial overlap is also observed for the same l_o curves.

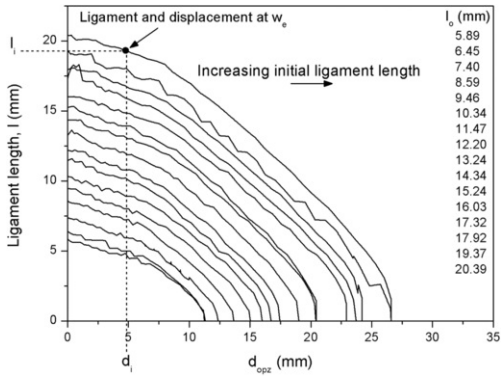

Fig. 6 Registered l versus d_{opz} curves for the 16 femtolaser specimens.

alt-text: Fig. 6

Eq. (2) can be evaluated as explained before. In Fig. 7, w_f as a function of l_o is represented, using, d_z and d_{opz}, two different ways of measuring the displacements. The w_e values, 127.05 ± 12.64 kJ/m^2 (d_z) and 130 ± 9.59 kJ/m^2 (d_{opz}), are practically coincident but the slopes, 21.35 ± 0.90 MJ/m^3 (d_z) and 19.94 ± 0.70 MJ/m^3 (d_{opz}), change slightly.

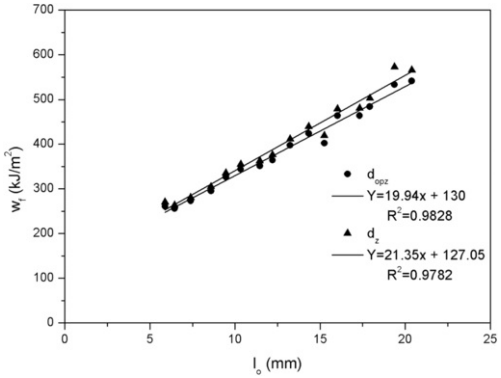

Fig. 7 EWF plot for the 16 femtolaser specimens: ●) Displacement d_{opz}, ▲) Displacement d_z.

alt-text: Fig. 7

The d_{opz} was measured using two reference points closely located to the OPZ, and in this way the OPZ was contained within these two points, for all specimens. The distance between these reference points was constant for all specimens. The displacements at rupture measured from the crosshead (d_z) are larger than the displacements measured from the limits defined by the outer plastic zone (d_{opz}). The elastic deformation outside the plastic zone is recovered on unloading so that both rupture displacements would be expected to be equal at least that the total recovery of other displacements, as viscoelastic, does not happen before specimen rupture.

Once w_e, σ_y, and E were obtained, the r_p was calculated and Eqs. (3)–(5) were accomplished. Thus, two of the key assumptions of the EWF are satisfied, i. e., the ligament length is completely yielded prior to the onset of crack initiation, and fracture is under plane stress conditions.

If the load in Fig. 5 is divided by the area of its initial ligament, a stress versus d_{opz} representation is obtained. This new plot is represented in Fig. 8. The hatched area under the σ-d_{opz} curves is equal to w_e = 130 kJ/m^2. A set of overlapping curves (heads) can be observed in the low displacement range up to a fairly recognizable value, d_i, from which the curves (tails) start to diverge. The hatched area begins at d_{opz} = 0 until the displacement d_i, where the crack initiation begins. When the displacements are larger than d_i then there is crack propagation. From the analysis of Fig. 8 the crack initiation displacement d_i = 4.94 ± 0.11 mm, the maximum stress σ_{max} = 28.75 ± 0.74 MPa, and the crack initiation stress σ_i = 25.89 ± 0.46 MPa can be identified.

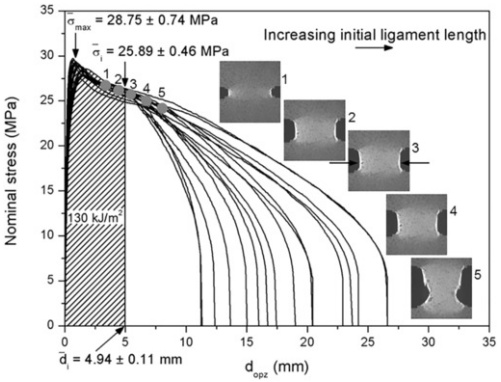

Fig. 8 Stress versus d_{opz} curves for the 16 femtolaser specimens.

alt-text: Fig. 8

The σ_{max} values are between σ_y and 1.15 σ_y and therefore Eq. (6) is also valid for all specimens. The Clutton and Hill criteria are now satisfied.

In Fig. 8 some of the frames registered by the DIC cameras are also schematised. The exact frame where crack initiation begins cannot be visually detected, but the arrows in the frame of Fig. 8 show that in this frame the crack

initiation has been initiated. The frames displayed in Fig. 8 indicate that prior to d_i there is no crack propagation and afterwards, the crack growth has already begun. The crack initiation corresponds very well with coordinates (d_i, σ_i), confirming the onset of crack initiation. Then, w_e is the specific energy just up to crack initiation. The frames in Fig. 8 follow a sequence of events leading to fracture of the DENT specimens. The process begins with the opening and blunting of the notch and the yielding of the ligament area, followed by crack initiation and propagation until complete failure.

The crack tip opening displacement at the onset of crack initiation, CTOD is

$$d_r = CTOD + \alpha \cdot l_o \quad \textbf{(7)}$$

where d_r is the displacement at complete rupture.

In Fig. 9 the obtained d_r values (Fig. 2) in front of l_o are plotted for the 16 specimens. A simple linear regression analysis of this plot shows that the CTOD value is the intercept for a zero ligament length. The CTOD value of 4.94 mm is coincident with d_i the displacement at the onset of crack initiation (Fig. 8).

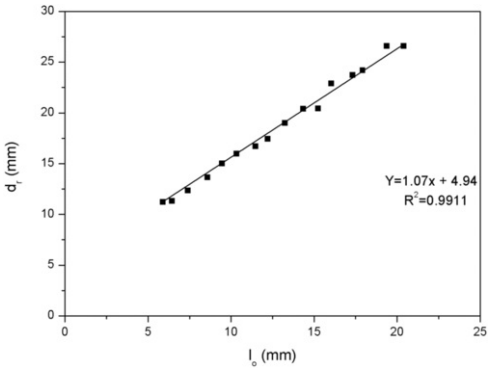

Fig. 9 Determination of CTOD for the 16 femtolaser specimens.

alt-text: Fig. 9

The crack length increment due to blunting, Δa_b, just prior to crack initiation is given (Fig. 1) by

$$\Delta a_b = l_o - l_i \quad \textbf{(8)}$$

where l_i is the ligament length at the onset of crack initiation. When l_i is represented as a function of l_o, there is a linear dependence between the two variables. The l_i values can be determined in Fig. 6 from the d_i values corresponding to each l_o specimen. In Fig. 10 the l_i values obtained for each l_o specimen are graphed. A simple linear regression on this graph results in an intercept Δa_b = 1.42 mm and a slope of 1, as predicted.

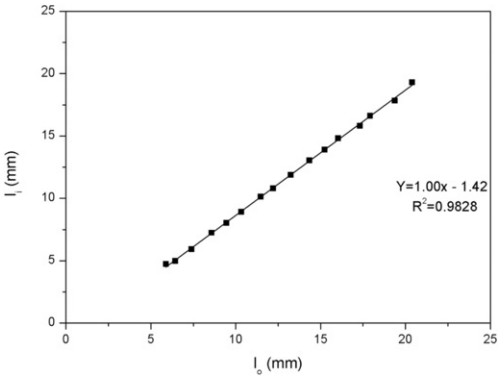

Fig. 10 Determination of Δa_b for the 16 femtolaser specimens.

alt-text: Fig. 10

To ensure that the fracture mechanism is the same, irrespective of the ligament length, the specimens must show a common and steady fracture phenomenology during crack growth.

In Fig. 6, the crack growth is comprised between the CTOD and d_r values. The crack growth range of Fig. 6 can be normalised using the Δa_b and CTOD values. The normalised results can be represented in a plot like the one shown in Fig. 11. Here, all the curves overlap except for the specimens with l_o = 5.89 mm and l_o = 19.37 mm, which show slight deviations. In this way the same two specimens are identified, which also have deviations in Figs. 5 and 6.

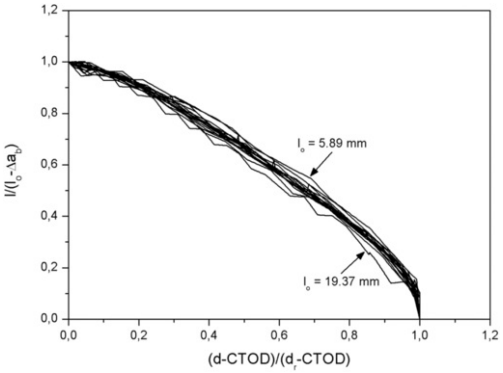

Fig. 11 Normalisation of crack growth for the 16 femtolaser specimens.

alt-text: Fig. 11

These two specimens were excluded and all the work was recalculated. At the end of the new analysis (w_e = 128.81 kJ/m^2 and βw_p = 19.87 MJ/m^3 using d_{opz}), the influence of these two specimens on the previous results was insignificant.

Now, the last of the key assumptions is satisfied because the remaining 14 specimens had repetitive sharp notches without plastic deformation ahead of the crack tip. As such, w_e is an inherent material property.

During the crack propagation, the load P versus the crack length a [2] is represented by

$$P = t\,(W - a)\,\sigma_i \tag{9}$$

and its derivative

$$\frac{dP}{da} = -t\sigma_i \tag{10}$$

Thus, if P is represented as a function of a, a straight line with slope $-t\sigma_i$ should be found.

The crack length (Fig. 1) is given by

$$a = W - l \tag{11}$$

Then, by combining Eq. (11) with Figs. 5 and 6, P as a function of a is depicted in Fig. 12 for the tails. The two curves that deviated from the others in Fig. 12 are directly related to the two previously discarded specimens. The linear dependence indicates that all propagations follow the same trend except at the higher a values, near the complete specimen fracture, where the slope increases. From the slope calculated of the 14 valid specimens, it is found that σ_i = 25.20 ± 0.96 MPa, which agrees with the previously determined value in Fig. 8.

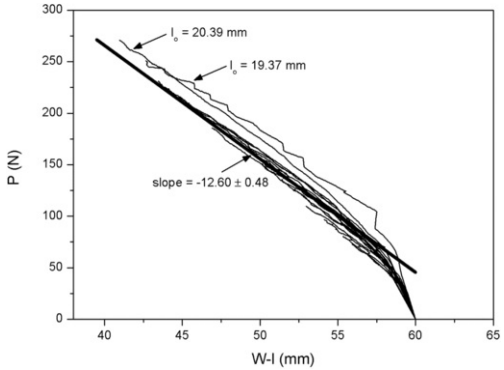

Fig. 12 Load versus a for the 16 femtolaser specimens.

alt-text: Fig. 12

The J-integral concept represents an energy contour path integral that is independent of the path around the crack. The J-integral can be represented [9] as

$$J = -\frac{1}{t}\left(\frac{dU}{da}\right)_{d=\text{constant}} \quad \textbf{(12)}$$

where U is the external work done up to a given constant displacement d, and a is the crack length. The Landes and Begley experimental method [9] is used here. This method requires two steps. The first step consists of the graphical representation of the energy divided by t, as a function of a, when d is fixed. The resultant plot is shown in Fig. 13. The points belonging to the same displacement show linearity and can be fitted by a straight line. By Eq. (12), the resultant slope of the regression line is -J. The second step consists of plotting the J values versus displacement, as illustrated in Fig. 14.

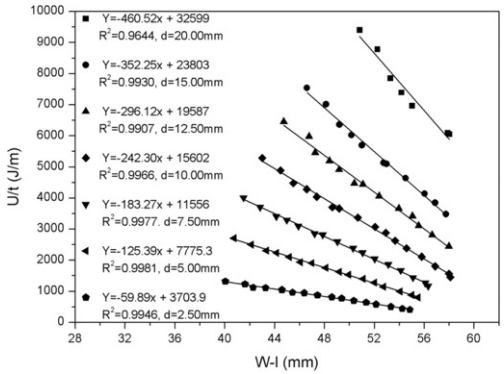

Fig. 13 Input energy divided by thickness versus a for the 14 valid femtolaser specimens.

alt-text: Fig. 13

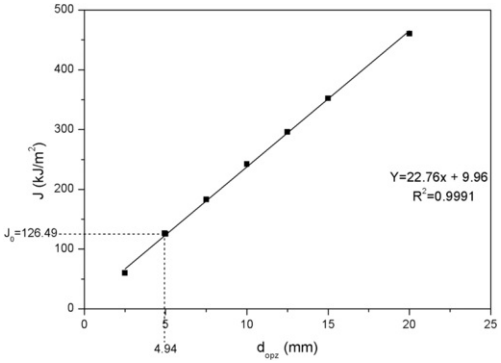

Fig. 14 J-integral plot for the 14 valid femtolaser specimens.

alt-text: Fig. 14

For a non-work hardening material and full yielding of the ligament [2], U/t is a linear function of a at a constant displacement, as it has been verified, then

$$J = \sigma_i \cdot d \quad \textbf{(13)}$$

In Fig. 14, the slope of the regression line, σ_i = 22.76 MPa, agrees reasonably well with the previously found σ_i values. The J value at crack initiation, J_o, is obtained by introducing the CTOD value in the J-integral plot, as shown in Fig. 14. This provides a value of J_o = 126.49 kJ/m^2 that matches well with w_e.

The relationship between J_o or w_e and CTOD given [2] by

$$J_o = \sigma_y \cdot CTOD = w_e \quad \textbf{(14)}$$

is satisfied.

4.4 Razor blade specimens

The load versus d_{opz} curves determined during testing are shown in Fig. 15 for each of the 16 specimens tested. Here, there is no overlap of curves observed.

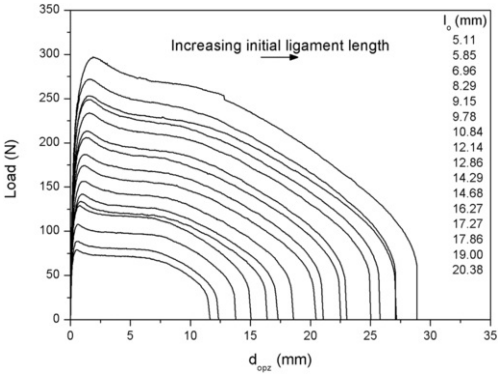

Fig. 15 Registered load versus d_{opz} curves for the 16 razor blade specimens.

alt-text: Fig. 15

Fig. 16 accounts for the registered data of l as a function of d_{opz}. A partial overlap of the specimens with l_o = 19 mm and l_o = 17.86 mm is observed.

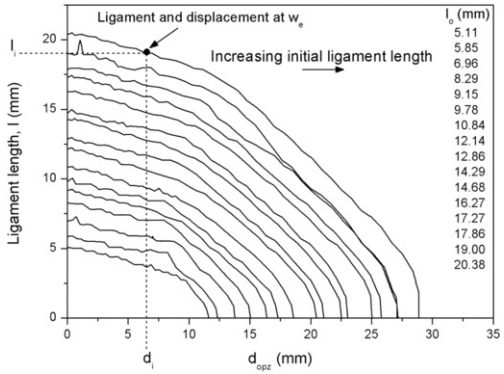

Fig. 16 Registered l versus d_{opz} curves for the 16 razor blade specimens.

alt-text: Fig. 16

The EWF plot of the 16 specimens, when d_{opz} is used, is displayed in Fig. 17. The intercept at $d_{opz} = 0$ of the regression line yields $w_e = 175.97$ kJ/m^2.

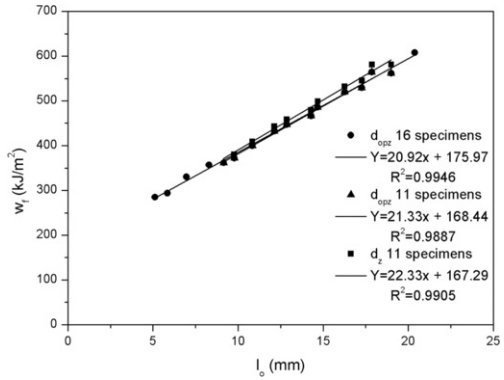

Fig. 17 EWF plot for the razor blade specimens: ●) d_{opz} 16 specimens, ▲) d_{opz} 11 specimens, ■) d_z 11specimens.

alt-text: Fig. 17

The stress versus d_{opz} curves are depicted in Fig. 18a. Two different populations of curves can be observed. One population has the 4 specimens with the shorter l_o specimens, while the other one contains the remaining 12 specimens.

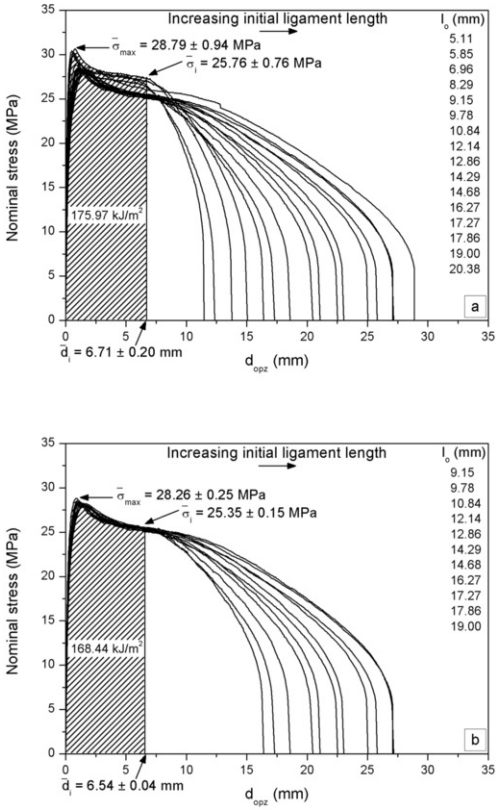

Fig. 18 Stress versus d_{opz} curves for the razor blade specimens: a) 16 specimens, b) 11 specimens.

alt-text: Fig. 18

For this case, the mean value of σ_{max} (Fig. 18a) surpasses the upper limit of the Hill criterion. The σ_{max} values for the 4 shorter l_o are larger than 1.15 σ_y, indicating the possibility that they could be in a mixed mode state. However, this is not the case because the shorter femtolaser specimens, which have similar l_o, were in a pure plane stress state. The Clutton criterion (Eq. (6)) is satisfied.

To investigate whether the fracture mechanism is the same for all the 16 specimens, it is convenient to perform the study of crack growth range, as was done before (Fig. 11) for the femtolaser specimens. The CTOD and Δa_b values were determined through Figs. 19 and 20, respectively. Now, with Δa_b and CTOD, the crack growth range of these specimens can be normalised. In Fig. 21 the normalised curves are represented. It can be clearly observed that 11 specimens overlap, 4 specimens present large deviations (l_o = 5.11 mm, l_o = 5.85 mm, l_o = 6.96 mm and l_o = 8.29 mm), and the specimen with l_o = 20.38 mm has a slight deviation.

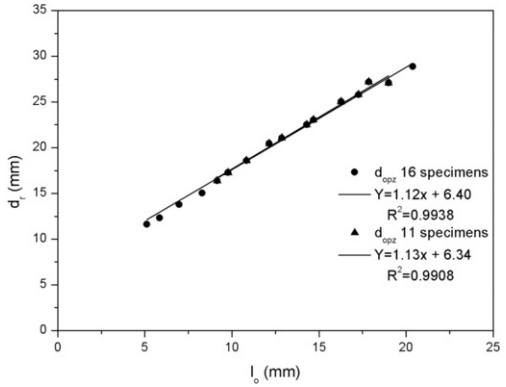

Fig. 19 Determination of CTOD for the razor blade specimens: ●) d_{opz} 16 specimens, ▲) d_{opz} 11 specimens.

alt-text: Fig. 19

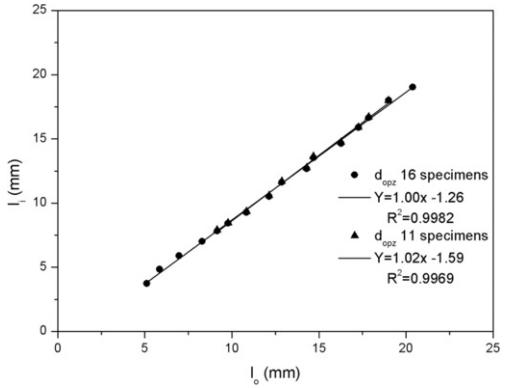

Fig. 20 Determination of Δa_b for the razor blade specimens: ●) d_{opz} 16 specimens, ▲) d_{opz} 11 specimens.

alt-text: Fig. 20

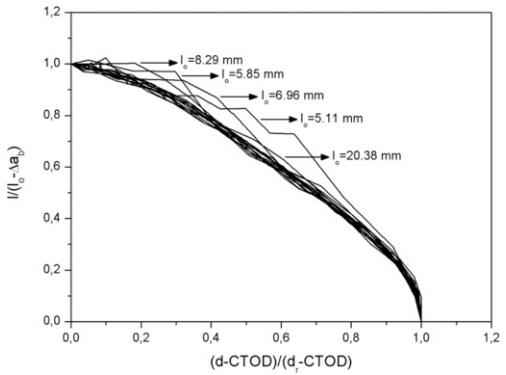

Fig. 21 Normalisation of crack growth for the 16 razor blade specimens.

alt-text: Fig. 21

The frames collected by the DIC system of these 5 specimens were carefully examined. In the 4 specimens with the shorter l_o, it is observed that the two notches of the same specimen do not initiate the propagation at the same time. This fact has been also seen in other polymer films [2,3] and can be originated by quality differences between the two notches of the specimen. Such differences are probably produced during the sliding of the razor blade in specimens with short l_o, being more difficult to sharpen that in specimens with large l_o value.

Intentionally, one specimen has been prepared using a different compressive component of the razor blade sliding force on the two notches. Fig. 22 shows the optical micrographs of both notches. Here, the different extent of plastic deformation can be observed. A frame of the tested specimen showing the non-simultaneous propagation of both cracks is also shown.

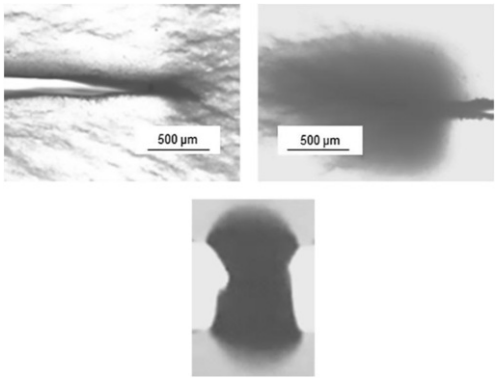

Fig. 22 Non-simultaneous crack propagation.

alt-text: Fig. 22

The only one difference observed in the specimen with lo = 20.38 mm, when compared with the other 11 valid specimens, was that a longer time was required for crack initiation. This can also be observed in Fig. 18a where its d_i value is larger than other specimens. The d_i value corresponds to an initiation stress of 25.35 MPa. Both notches propagate at the same time, but their comparatively larger displacement and longer time to crack initiation can be attributed to either their larger crack tip radius, or the increased plastic deformation ahead of the crack tip, despite the parity of the notch quality, when compared to the other 11 valid specimens.

Now, after discarding the 5 anomalous specimens, the work was entirely recalculated with the 11 valid specimens. These specimens satisfied Eqs. (3)–(5) and two of the key requirements were fulfilled, i.e., the ligament lengths are completely yielded prior to the onset of crack initiation and fracture is under plane stress conditions. However, in spite of the repetitive sharp notches, these specimens have plastic deformation ahead of the crack tip, and therefore the third key requirement is not accomplished. Thus, w_e with a value equal to 168.44 kJ/m^2 is not an inherent material property.

The EWF plot of the 11 valid razor blade sharpened specimens is depicted in Fig. 17 for the measured displacements d_z and d_{opz}. The w_e values for both displacements are practically identical, 167.29 ± 10.49 kJ/m^2 (d_z) and 168.44 ± 10.91 kJ/m^2 (d_{opz}), but the slopes change slightly, 22.33 ± 0.73 MJ/m^3 (d_z) and 21.33 ± 0.76 MJ/m^3 (d_{opz}), as in the femtolaser specimens (Fig. 7). The w_e = 168.44 kJ/m^2 for the 11 specimens is slightly less than the w_e = 175.97 kJ/m^2 obtained from the 16 specimens.

In Fig. 18b the curves σ versus d_{opz} are represented for the 11 valid specimens. The σ_{max} is 28.26 ± 0.25 MPa, and each σ_{max} value meets Hill and Clutton criteria. The hatched area under the σ-d_{opz} curves is equal to 168.44 kJ/m^2 (w_e value). This hatched area begins at d_{opz} = 0 and extends until d_i = 6.54 ± 0.04 mm. In this low range of displacements, all the curves (heads) overlap. From d_i, the curves (tails) start to diverge until d_r. So, in Fig. 18b, d_i is identified as the displacement at the onset of crack initiation and its corresponding stress value, σ_i = 25.35 ± 0.15 MPa, as the stress at the onset of crack initiation. This behaviour has been previously found [2,3] for razor blade and femtolaser sharpened specimens.

The CTOD value (6.34 mm) is determined in Fig. 19. As expected, this value is coincident with the d_i value identified in Fig. 18b, and Δa_b = 1.59 mm is obtained in Fig. 20 for the 11 specimens.

Proceeding as before with the femtolaser specimens; the load during the crack propagation is represented in Fig. 23 for each one of the 16 tested razor blade sharpened specimens. Discarding the 4 shorter l_o specimens, and the specimen with l_o = 20.38 mm, a straight line as predicted by Eq. (10), results. The 5 curves that depart from the other in Fig. 23 correspond to the 5 specimens discarded before. By applying Eq. (10) to the slope of the straight line obtained from the 11 valid specimens shown in Fig. 23, it is found that σ_i = 25.06 ± 0.88 MPa, a value that agrees very well with the σ_i values determined before.

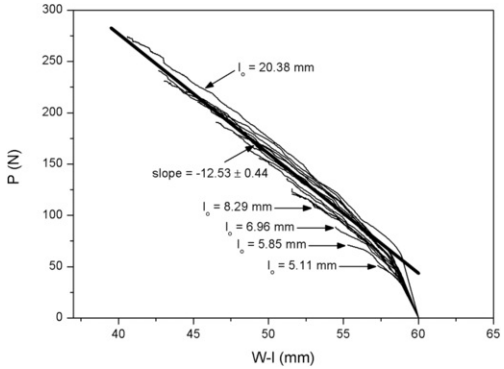

Fig. 23 Load versus a for the 16 razor blade specimens.

alt-text: Fig. 23

The J-integral procedure was performed as described before. The two steps of the experimental method are shown in Figs. 24 and 25. In Fig. 24, the points belonging to the same displacement show linearity and can be fitted by a regression line. The slope of this line is -J (Eq. (12)). These slopes are displayed in Fig. 25 as a function of the displacement. Here, following Eq. (13), the slope of the regression line σ_i results in 22.04 MPa, which agrees reasonably with the σ_i value encountered in Fig. 18b. Using the displacement at the onset of crack initiation gives J_o = 166.01 kJ/m^2, which also agrees with w_e.

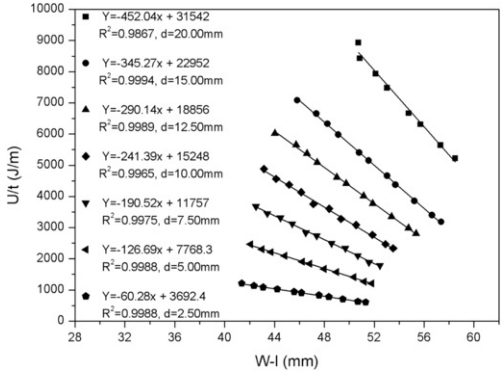

Fig. 24 Input energy divided by thickness versus a for the razor blade specimens.

alt-text: Fig. 24

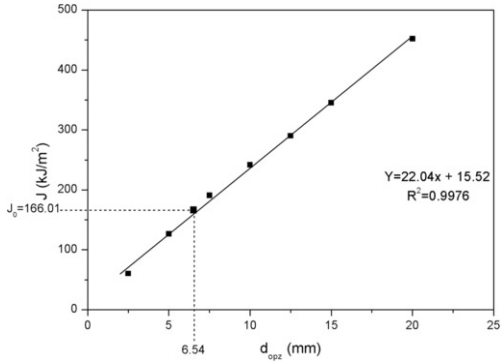

Fig. 25 J-integral plot for the razor blade specimens.

alt-text: Fig. 25

The 11 selected specimens have repetitive sharp notches, but with plastic deformation ahead of the notch tip, this set of specimens does not fulfil the key requirement of consistent, high quality notches. As a consequence, w_e is not an inherent material property. However, the relationship between w_e, J_o, CTOD and σ_i, given by Eq. (14), is completely fulfilled. These values depend on the notch quality and their relationships are maintained.

4.5 Femtolaser versus razor blade

There are differences in the notch quality between the femtolaser and the razor blade sharpened specimens. The plastic deformation leads to higher values of w_e, CTOD and J_o, although their values successfully accomplish Eq. (14).

In polymer films [2,3] less ductile than EPBC, it has been possible to generate notches using the razor blade sliding technique with and without plastic deformation in front of the notch tip. Once specimens containing plastic deformation were discarded, the fracture parameters were coincident with those obtained in femtolaser specimens.

The mean σ_{max} and σ_i values for the femtolaser and razor blade specimens have the same values. However, the CTOD and Δa_b values are larger for the razor blade sharpened specimens.

For a more thorough analysis of the σ-d_{opz} curves, in Fig. 26a the registered curves obtained from two equal ligament lengths are displayed, one sharpened by femtolaser and the other by razor blade. For the same specimens, the l-d_{opz} curves are shown in Fig. 26b. In Fig. 26a and b can be observed that the d_r value is larger for the razor blade sharpened specimen. Another way to represent these data can be performed by shifting the σ-d_{opz} and l-d_{opz} curves along the displacement axis so that the rupture displacements coincide, as shown in Fig. 27a for the σ-d_{opz} curves and in Fig. 27b for the l-d_{opz} curves. Doing so, the d_i values fall in the same place, and the tails overlap. With such representation, it can be deduced that the crack growth, and the propagation energy, are the same for both sharpening methods, and then the slope βw_p of the EWF plot would have the same value for both sets of specimens, as is observed. In Fig. 26a, it can be seen that the two curves overlap in the range comprised between the displacements $d_{opz} = 0$ and the displacement corresponding to σ_{max}. In Fig. 27b, it can be observed that the tails also overlap. The difference between both curves occurs in the range comprised between the displacement corresponding to σ_{max} and d_i. In spite of this, σ_i is the same for both notch sharpening procedures.

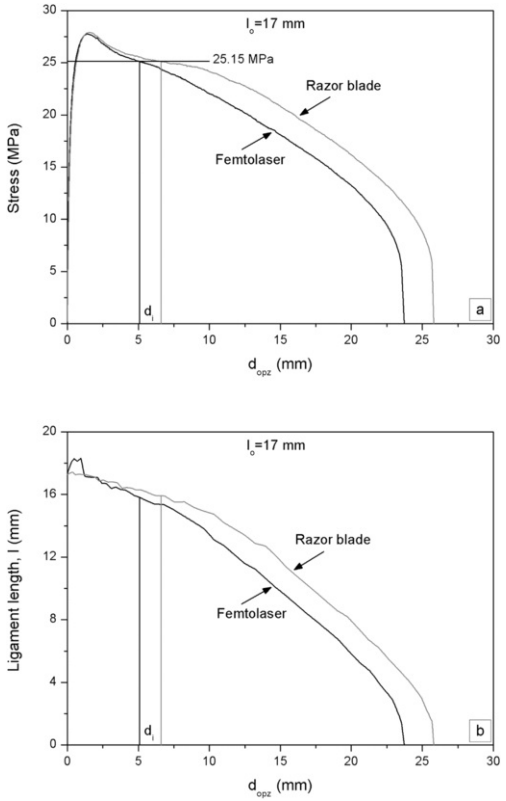

Fig. 26 Femtolaser and razor blade specimens with l_o = 17 mm: a) σ versus d_{opz}, b) l versus d_{opz}.

alt-text: Fig. 26

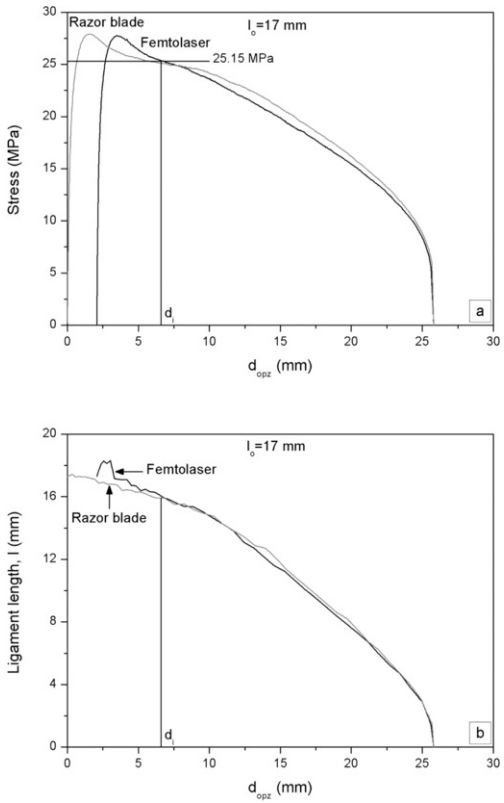

Fig. 27 Femtolaser and razor blade specimens with l_o = 17 mm: a) Shifted σ-d_{opz}, b) Shifted l-d_{opz}.

alt-text: Fig. 27

The same trends have been observed in other ductile polymer films [2,3]. It is clear that the shape of the stress-displacement curves is greatly influenced by the quality of the notches.

If there is a set of specimens with the same notch tip radius, but has some specimens with, and others without, plastic deformation ahead of the notch tip, then, after testing, all specimens would have the same σ_{max} and σ_i but different d_i. This results in crossing curves in the load-displacement and ligament length-displacement plots. These behaviours can be expected if the set contained specimens that had different levels of plastic deformation.

The normalised crack growth versus displacement curves of the crack propagation are shown in Figs. 11 and 21 for the femtolaser and razor blade specimens, respectively. If a single graph of both figures is made, after discarding the non-valid specimens, all the curves will overlap, confirming that both sets of specimens present the same propagation behaviour. The normalised plots of the crack growth versus displacement are helpful to reject those specimens with different quality notches.

This EPBC grade presents w_e values of 130 and 168.44 kJ/m^2 for the femtolaser and razor blade sets of specimens, respectively. Their βw_p value is approximately 21 MPa/m^3, considering an average of the different ways to measure the displacement. Martínez et al. [6] found w_e values of 60 and 116 kJ/m^2 for two sets of femtolaser and razor blade specimens, respectively, and an average βw_p value of approximately 15 MJ/m^3, for another EPBC grade, which had the same 8.5% ethylene content but a lower molecular weight. Thus, the increase in molecular weight results in an increase in toughness and in propagation energy.

4.6 The shape of the stress-displacement curves

The shape and size of the stress-displacement curves obtained from specimens that were notched in different ways, makes it possible to analyse their EWF behaviour when they are compared with the two previously analysed sets of specimens, the femtolaser and the razor blade sharpened specimens.

Four new specimens have been manufactured. The first of these specimens was sharpened by applying the razor blade sliding technique, but, in this case, the sharpening was carried out over specimens that were frozen in liquid nitrogen, that is, below the T_g of the material. Reduction of the plastic deformation ahead of the notch tip is expected when it is compared with the razor blade sharpened notches at room temperature. Then, equal values of σ_{max} and σ_i will be anticipated, unlike the femtolaser and razor blade (room temperature) sharpened specimens, and also equal tails of the stress-displacement curves. However, intermediate values for d_i and d_r are also expected, resulting in an intermediate w_e value.

Fig. 28a shows the registered stress-displacement curves for 3 specimens with similar l_o values. The curve F corresponds to l_o = 11.47 mm femtolaser specimen, the curve G corresponds to l_o = 10.84 mm razor blade (room temperature) sharpened specimen, and the curve N_2 corresponds to l_o = 10.41 mm razor blade (liquid nitrogen) sharpened specimen. Fig. 28b shows the same curves of Fig. 28a but shifted to the same d_r. As expected, the 3 curves have the same σ_{max}, σ_i, and tails, but the d_i, the CTOD, increases with the plastic deformation, resulting in higher w_e values.

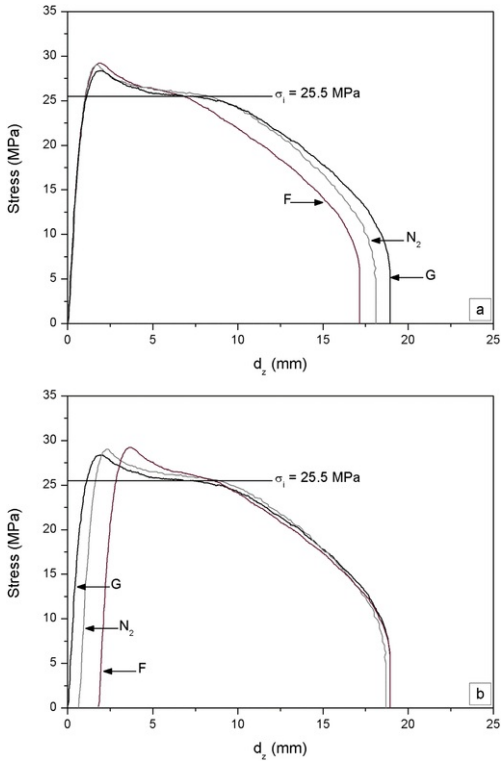

Fig. 28 Stress-displacement curves for F-femtolaser (l_o = 11.47 mm), G-room temperature razor blade (l_o = 10.84 mm), and N_2-liquid nitrogen razor blade (l_o = 10.41 mm): a) Measured displacement, b) Displacement shifted to d_r.

alt-text: Fig. 28

Whereas the two edge notches were properly aligned in all the tested specimens, in the second of the 4 new specimens, the two edge notches, sharpened by razor blade sliding, were not collinear. Instead, they had 1 mm separation. The non-collinearity of the two edge notches can modify the stress distribution in the ligament zone, and the results will likely be influenced. In Fig. 29, the stress-displacement curve registered for this specimen (l_o = 12.28 mm) with non-collinear notches is presented. For comparison purposes, a razor blade sharpened specimen with collinear notches and l_o = 12.31 mm is also presented. These 2 curves show equal σ_{max} values and overlap between $d_z = 0$ and $d_z = d_i$. If equal σ_i values (25.5 MPa) are also considered for both curves, equal w_e values are implied. However, the curve of the specimen with non-collinear notches has a larger d_r value, causing that the tails of both curves do not overlap. Further, the area of the σ-d_z curve between d_i and d_r is also larger, causing βw_p to be higher for the specimen with non-collinear notches.

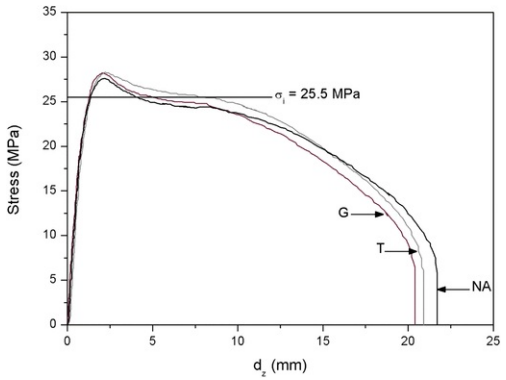

Fig. 29 Stress-displacement curves for G-razor blade collinear notches (l_o = 12.31 mm), NA-razor blade non-collinear notches (l_o = 12.28 mm), and T-tilted razor blade collinear notches (l_o = 12.13 mm).

alt-text: Fig. 29

The specimens have to be tested with the direction of tension perpendicular to the collinear notches. That is, the specimens must be properly mounted on the grips of the testing machine. If the specimens are tilted when they are mounted on the grips, then the collinear notches of the specimen are not oriented perpendicularly to the direction of tension, and so the stress distribution in the ligament is modified. The third of the 4 new specimens, a razor blade sharpened specimen with l_o = 12.13 mm, has been tested with the specimen tilted by 5° on the grips. Its stress-displacement curve is shown in Fig. 29 and could be compared to the specimen with l_o = 12.31 mm, which was correctly mounted on the grips. The curves for these two specimens overlap only up to σ_{max}. After this point, the curve of the tilted specimen is greater and has a larger d_r value than the non-tilted specimen. Considering σ_i = 25.5 MPa, the tilted specimen will have a higher w_e value than the properly mounted specimen.

In order to study the influence of the notch tip radius on the stress-displacement curves, circular holes were drilled to use as notches. The pressure exercised by the drill bit at the beginning caused a very large plastic deformation that extended to the material outside the hole, especially for small diameter holes. After several attempts, a specimen (l_o = 12.26 mm) with two edge holes (diameter ϕ = 2 mm) that had the same level of plastic deformation in both holes was obtained. To obtain the notches the drilling was followed by opening the two edge notches. The last of the 4 new specimens was tested, and the experimental stress versus displacement curve is represented in Fig. 30a. For comparison purposes, the curves for the femtolaser (l_o = 12.20 mm) and razor blade (l_o = 12.14 mm) specimens are also presented in this figure. In Fig. 30a can be observed that the 3 curves overlap just up to σ_{max}. From this point forward, the drilled specimen showed larger values for the stress and for d_r. The same stress-displacement curves of Fig. 30a were shifted along the displacement axis so that the rupture displacements were the same, and are represented in Fig. 30b. Considering σ_i = 25.5 MPa for the drilled specimen obtained from the femtolaser and razor blade specimens, as represented in Fig. 30a and b, it could be inferred that the drilled specimen will have higher w_e, Δa_b, and CTOD values, while the tail region seems to be quite similar to the other curves. In any case, the influence of the notch tip radius on the fracture parameters is clear.

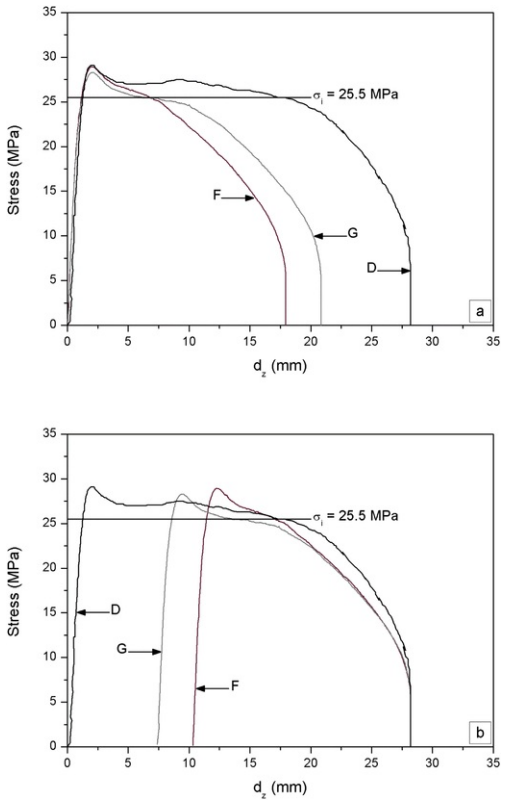

Fig. 30 Stress-displacement curves for F-femtolaser (l_o = 12.20 mm), G-razor blade (l_o = 12.14 mm), and D-drilled (l_o = 12.26 mm): a) Measured displacement, b) Displacement shifted to d_r.

alt-text: Fig. 30

5 Conclusions

The femtosecond laser ablation technique enables obtaining very consistent, sharp notches, without plastic deformation ahead of the notch tip. This notch sharpening technique is the most appropriate to sharpen notches of the most ductile films and gives the lowest values for the fracture parameters. The limitations include the availability of the equipment and the high cost per notch.

Notch sharpening using the classic razor blade sliding technique can yield notches with different quality, which depends on the material ductility and the compressive component of the sideways sliding force that is applied. Sharp notches without plastic deformation can be obtained, and will yield values similar to the femtolaser specimens. Normally, however, specimens with plastic deformation ahead of the notch tip are obtained. When the two notches of the same specimen have different levels of plastic deformation, the crack initiation does not occur at the same time. Specimens with different levels of plastic deformation can be obtained. Variability in the same laboratory and between different laboratories of the w_e, J_o, and CTOD values can be explained by the different levels of plastic deformation ahead of the notch tip or the notch tip radius that can be generated by operators when sharpening the notches. The larger the level of plastic deformation, the larger will be the displacement at initiation, resulting in higher values of Δa_b and w_e. However, as the propagation does not depend on the plastic deformation, the same βw_p value will be obtained.

It is confirmed that a key requirement to obtain meaningful results is to have consistent notches without plastic deformation in front of the notch root. The notch tip radius has a strong influence on the fracture parameters.

The shape of the stress-displacement curves depends on the notch quality. Consistent notches have the same σ_{max}, σ_i, d_i, CTOD, and Δa_b values, and then the normalised curves of the propagation region overlap. Non-overlapping curves belong to specimens with different quality notches and can be discarded.

The w_e, J_o, and CTOD values obtained from specimens with plastic deformation at the crack tip, being this the only key assumption not accomplished, satisfy the relationships among w_e, CTOD, J_o, and σ_i, but these values are

not inherent properties of the material.

The inspection of the notches in a light optical microscope before testing could be helpful to detect plastic deformation in front of the crack tip.

Non-collinear notches and misalignment of the specimens on the grips, affect the stress-displacement curves and the results. Small differences of less than 1 mm in the collinearity of the notches can be unintentionally generated during the specimen manufacture and have a small effect on the results. More care is necessary when mounting the specimens on the grips because the shape of the stress-displacement curve is more affected and thus the results. Specimens with non-collinear notches and incorrectly aligned can also be detected by normalising the curves in the propagation region.

The EWF approach has been successfully applied on an EPBC. This heterophase polymer has multiple shear yielding as a deformation mechanism, which is different from polymers that undergo necking before the onset of crack propagation. In EPBC, given the same ethylene content, the fracture energy increases as the average molecular weights increase.

Acknowledgements

The authors acknowledge the Ministerio de Economia y Competitividad of Spain for its financial support through the research project MAT2012-37762-C02-01. N. León expresses his gratitude to the National Council for Science and Technology (CONACYT, Mexico) for the predoctoral fellowship.

References

[1] B. Cotterell and J.K. Reddel, The essential work of plane stress ductile fracture, *Int. J. Fract.* **13**, 1977, 267–277.

[2] A.B. Martínez, N. León, D. Arencón and M. Sánchez-Soto, Essential work of fracture, crack tip opening displacement, and J-integral relationship for a ductile polymer film, *Polym. Test.* **55**, 2016, 247–256.

[3] A.B. Martínez, N. León, D. Arencón and M. Sánchez-Soto, The post-yield fracture of a ductile polymer film: notch quality, essential work of fracture, crack tip opening displacement, and J-integral, *Eng. Fract. Mech.* **173**, 2017, 21–31.

[4] E. Clutton, Essential work of fracture, In: D.R. Moore, A. Pavan and J.G. Williams, (Eds.), *Fracture Mechanics Testing Methods for Polymers, Adhesives and Composites,* 2001, Elsevier Science, Ltd.; Oxford, 177–195.

[5] J.G. Williams and M. Rink, The standardisation of the EWF test, *Eng. Fract. Mech.* **74**, 2007, 1009–1017.

[6] A.B. Martínez, A. Segovia, J. Gamez-Perez and M.L. Maspoch, Influence of femtolaser notch sharpening Technique in the determination of essential work of fracture (EWF) parameters, *Eng. Fract. Mech.* **76**, 2009, 1247–1254.

[7] R. Hill, On discontinuous plastic states, with special reference to localized necking in thin sheets, *J. Mech. Phys. Solids* **1**, 1952, 19–30.

[8] A.B. Martínez, D. Arencón, J. Rodríguez and A. Salazar, Influence of the notch sharpening on the impact fracture toughness of ethylene-propylene block copolymers, *Polym. Test.* **36**, 2014, 75–81.

[9] J.A. Begley and J.D. Landes, The J integral as a fracture criterion, In: *Fracture Toughness, ASTM STP 514,* 1972, American Society for Testing and Materials; Philadelphia, 1–20.

Queries and Answers

Query: Please note that author's telephone/fax numbers are not published in Journal articles due to the fact that articles are available online and in print for many years, whereas telephone/fax numbers are changeable and therefore not reliable in the long term.
Answer: I agree with your observation.

Query: Please provide the grant number for 'National Council for Science and Technology (CONACYT, Mexico)' if any?
Answer: There is no grant number associated.

Query: Please confirm that given names and surnames have been identified correctly and are presented in the desired order and please carefully verify the spelling of all authors' names.
Answer: They are all correct.